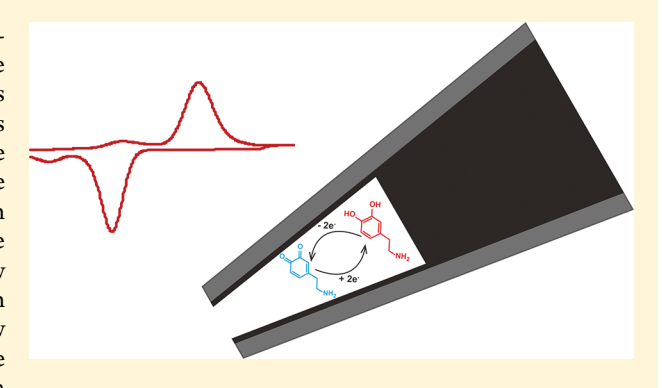


Cavity Carbon-Nanopipette Electrodes for Dopamine Detection

Cheng Yang, ** Keke Hu, **, * Dengchao Wang, ** Yasmine Zubi, * Scott T. Lee, * Pumidech Puthongkham, * Michael V. Mirkin, **, * and B. Jill Venton**

Supporting Information

ABSTRACT: Microelectrodes are typically used for neurotransmitter detection, but nanoelectrodes are not because there is a trade-off between spatial resolution and sensitivity that is dependent on surface area. Cavity carbon-nanopipette electrodes (CNPEs), with tip diameters of a few hundred nanometers, have been developed for nanoscale electrochemistry. Here, we characterize the electrochemical performance of CNPEs with fast-scan cyclic voltammetry (FSCV) for the first time. Dopamine detection using cavity CNPEs, with a depth equivalent to a few radii, is compared with that using open-tube CNPEs, an essentially infinite geometry. Open-tube CNPEs have very slow temporal responses that change over time as the liquid rises in the CNPE. However, a cavity CNPE has a fast temporal response to a



bolus of dopamine that is not different from that of a traditional carbon-fiber microelectrode. Cavity CNPEs, with tip diameters of 200-400 nm, have high currents because the small cavity traps and increases the local dopamine concentration. The trapping also leads to an FSCV frequency-independent response and the appearance of cyclization peaks that are normally observed only with large concentrations of dopamine. CNPEs have high dopamine selectivity over ascorbic acid (AA) because of the repulsion of AA by the negative electric field at the holding potential and the irreversible redox reaction. In mouse-brain slices, cavity CNPEs detected exogenously applied dopamine, showing they do not clog in tissue. Thus, cavity CNPEs are promising neurochemical sensors that provide spatial resolution on the scale of hundreds of nanometers, which is useful for small model organisms or for locations near specific cells.

Teurochemical detection in vivo has predominantly been performed with microelectrodes. Carbon-fiber microelectrodes (CFMEs), with diameters of 7 μ m and lengths of 50– 100 μ m, are the most popular electrodes for direct detection of electroactive species. Although these electrodes work well for measuring average changes in rodent brains, there are a variety of other applications that would benefit from robust and sensitive nanoelectrodes. Small-animal models such as Drosophila and zebrafish are easy to genetically manipulate, 1-3 but the small dimensions of their central nervous systems require better spatial resolution to implant the probe into a specific brain region.⁴⁻⁷ In addition, measurements of neurotransmitters are being made in single synapses, which require electrodes with nanosized tips, preferably in disk geometries.8 Carbon-nanofiber microelectrodes fabricated on large silicon chips have been developed for neurotransmitter detection, but the large dimensions of the chip and the geometry limit the implantation. Flame-etching or electrochemically etching carbon fibers can create finite conical nanoelectrodes with 50-200 nm tip diameters, but they are still micrometers in length.^{8,10} Etching requires nanoelectrodes to be fabricated individually, and reproducibility is poor. Robust, sensitive, and easy-to-fabricate

nanoelectrodes would enable many new types of experiments and play a crucial role in understanding neurotransmission and neuromodulation.11

Nanometer-scale pipettes pulled from borosilicate or quartz capillaries have been widely used in bioanalysis, 12 nanoelectrochemistry, 11 and scanning-probe microscopies. 13,14 Nanoscale-carbon-pipette electrodes are also useful for localized detection of neurotransmitters at the level of single cells, single vesicles, or single synapses. 8,9,11,15-17 For nanopipette electrodes, carbon is selectively deposited on the inner wall of a pulled capillary by chemical vapor deposition (CVD), resulting in controllable thickness of the carbon film. The process facilitates batch fabrication with high reproducibility. Takahashi et al. described the pyrolytic decomposition of carbon precursor gases inside pulled-quartz-glass nanopipettes, which produced nanometer carbon electrodes with small overall dimensions at the probe tip. 18 Carbon nanopipettes have been successfully utilized for injection of chemicals into living cells, 19 as ohmic

Received: December 21, 2018 Accepted: February 27, 2019 Published: February 27, 2019

[†]Department of Chemistry, University of Virginia, Charlottesville, Virginia 22904, United States

[‡]Department of Chemistry and Biochemistry, Queens College—CUNY, Flushing, New York 11367, United States

[§]The Graduate Center of the City University of New York, New York, New York 10016, United States

nanoelectrodes for intracellular electrophysiological recording of responses to pharmacological agents, ²⁰ and as nanoelectrodes for the measurement of reactive oxygen and nitrogen species in cells. ²¹ Our group has reported the application of small, robust, and sensitive closed-tip conical carbon nanopipettes (CNPEs) for the in vivo detection of endogenous dopamine release in *Drosophila* larvae. ¹⁵ Although the tip diameter is in the submicrometer range, the length is on the scale of tens of micrometers, which is controlled by etching the quartz away. Because the electrochemical signal is proportional to the surface area of the electrode, the balance between sensitivity (larger surface area) and spatial resolution (smaller detection dimensions) is always difficult, and nanoelectrodes have had limited applications in tissue.

The goal of this study was to characterize CNPEs that truly sample from a nanometer-sized region for the detection of neurotransmitters. CNPEs were made with either a cavity (i.e., a depth equivalent to a few pipette radii, also known as nanosamplers¹⁶) or open-tube (essentially infinite) geometry. The electrodes thus only sample at the tip, and the spatial resolution is equivalent to the diameter of the tip. However, the cavity or open-tube geometry provides a large active carbon surface area inside the nanoelectrode. We characterized CNPEs with open-tubes and cavity geometries with fast-scan cyclic voltammetry (FSCV)^{4,22} for the first time and found that cavity CNPEs have sufficient temporal resolution and sensitivity for dopamine. The small cavity traps and increases the local dopamine concentration, which improves currents, but the trapping does not slow the temporal response, which is on the order of seconds. High selectivity is observed for dopamine detection over ascorbic acid because of the enhanced electric field and the redox cycling for dopamine. Thus, cavity CNPEs are true nanoelectrodes that can provide spatial resolution in the hundreds of nanometers range, while still maintaining enough current to detect physiological levels of neurotransmitters.

■ EXPERIMENTAL SECTION

Electrochemistry. FSCV was performed with a Chem-Clamp potentiostat (Dagan, Minneapolis, MN, with a 1 MΩ headstage). The waveform was generated, and the data was collected using a high-definition-cyclic-voltammetry (HDCV) breakout box, an HDCV-analysis software program (UNC Chemistry Department, Electronics Design Facility, Chapel Hill, NC), and PCIe-6363 computer-interface cards (National Instruments, Austin, TX). Electrodes were backfilled with 1 M KCl, and a silver wire was inserted to connect the electrode to the potentiostat headstage. The typical triangular waveform swept the applied potential from -0.4 to 1.3 V at 400 V/s versus an Ag/AgCl reference electrode at a scan-repetition frequency of 10 Hz. The repetition rate was varied for some experiments.

Electrodes were tested using a flow-injection system, as previously described.²³ Analyte was injected for 5 s, and current-versus-time traces were obtained by integrating the current in a 100 mV window centered at the oxidation peak for each cyclic voltammogram (CV). Background-subtracted CVs were calculated by subtracting the average of 10 background scans taken before the compound was injected from the average of 5 CVs recorded after the analyte bolus was injected.

Carbon-Nanopipette-Electrode Fabrication. Nanopipettes were heat-pulled from quartz capillaries (1.0 mm outer diameter and 0.5/0.7 inner diameter, Sutter Instrument, Novato, CA), and their insides were coated with carbon by chemical vapor deposition (CVD) to yield open-tube or cavity

CNPEs. Specifically, nanopipettes with tip diameters of 200–400 nm were pulled using pulling programs based on HEAT = 650, FIL = 3, VEL= 22, DEL = 135, and PULL = 85. Cavity CNPEs were fabricated by 1 h CVD with methane and argon (1:1 ratio) at 945 °C, whereas open-tube CNPEs were fabricated by 45 min CVD with methane and argon (5:3 ratio) at 950 °C. All the parameters were adjusted slightly to obtain the required sizes and geometries.

Surface Characterization. A JEOL JEM-2100 transmission electron microscope (TEM) was used to characterize the carbon distribution near the tip of the CNPE. The CNPE was attached to the grid (PELCO Hole Grids, copper) in such a way that its tip was shown in the grid center hole, and the rest of the CNPE was cut off. A relatively low electron-beam voltage of 120 kV was used to reduce charge- and heat-accumulating effects on the glass layer.

Finite Element Simulation. The finite element simulation of the cavity carbon-nanopipette electrodes for dopamine detection was conducted using COMSOL Multiphysics 5.3a, and a detailed description of the simulation is in the Supporting Information. Briefly, following an earlier report, ^{1S} a 2D axisymmetric model was built to model the voltammogram of dopamine. The "Transport of Dilute Species" and "Electrostatics" modules were coupled to simulate the electrochemical processes and the electric double-layer structure at the carbon—solution interface. A time-dependent solver was used to simulate the cyclic voltammogram at a high potential-scan rate of 400 V/s.

Brain-Slice Experiments. Exogenous application of dopamine in mouse-brain slices was used to test the CNPE's performance in tissue. All animal experiments were approved by the Animal Care and Use Committee of the University of Virginia. C57BL/6 mice (6-8 weeks, Jackson Laboratories, Sacramento, CA) were housed in a vivarium and fed and given water ab libitum. The mice were anesthetized with isoflurane, sacrificed using cervical dislocation, and beheaded immediately. The brain was removed within 2 min and placed in chilled (0-5)°C) aCSF for 2 min; 400 μ m sagittal slices of the caudate putamen were prepared using a vibratome (LeicaVT 1000S, Bannockburn, IL), and transferred to oxygenated aCSF (95% O₂) and 5% CO₂) for 1 h prior to experimentation in order to reach equilibrium. The CNPE was inserted 75 μ m into the caudate putamen. The picospritzing micropipettes were made by pulling a 1.2×0.68 mm glass capillary (A-M Systems, Carlsburg, WA) using a vertical pipette puller (Narishige, Tokyo, Japan). The tip of the pipette was then trimmed to make an opening and marked in order to better visualize it in the tissue. Dopamine (150 μ M) was pressure-ejected into the brain slices using a Parker Hannifin picospritzer (Picospritzer III, Cleveland, OH). The picospritzing micropipette was placed 20-30 μ m from the CNPE. The picospritzing parameters were 20 psi for 0.02-1.50 s, which resulted in 5–268 nL of 150 μ M dopamine (0.8–40 pmol) being delivered into the tissue. The pipette was calibrated by ejecting dopamine solution into oil and measuring the diameter of the droplet; the volume of the spherical droplet was then calculated $(4/3\pi r^3)$, and the moles released were determined.

Statistics. All values are given as means \pm standard errors of the mean (SEM) for n electrodes, and all error bars are SEM. Paired or unpaired t tests were performed to compare properties between two groups. One-way ANOVAs with Bonferroni posttests were used to compare effects among multiple groups. All statistics were performed in GraphPad Prism6 (GraphPad Software, Inc., La Jolla, CA).

■ RESULTS AND DISCUSSION

Physical Characterization. Deposition of carbon inside quartz nanopipettes has been extensively studied, and deposition conditions have been optimized to produce different geometries with continuous inner carbon. 16,18,20,24–26 Figure 1

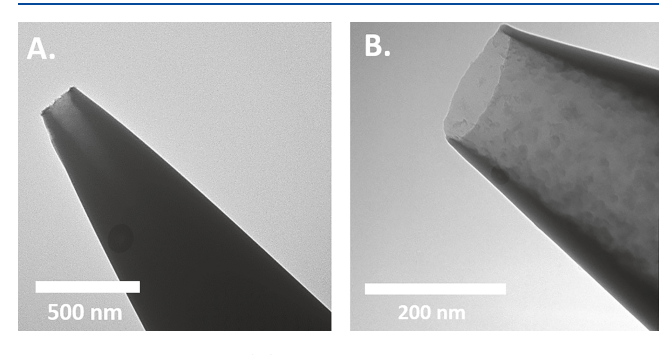


Figure 1. TEM image of (A) cavity CNPE with a cavity depth of about 500 nm and an orifice diameter of about 200 nm, and (B) open-tube CNPE with an orifice diameter of about 200 nm and a long depth.

shows TEM images of CNPEs with carbon-coated inner walls. The fabricated-CNPE geometry is generally described by the aspect ratio H = h/a, where h is the depth of the carbon-coated cavity, and a is the orifice diameter. Tip diameters were 200–400 nm, and although it is hard to precisely determine the depth of the cavity from TEM because of the glass thickness (Figure 1A), previous estimates with thinner glass show H = 12-30. In comparison, open-tube CNPEs have a similar tip diameter (~200 nm) but with an open channel in the middle, so the effective aspect ratio is larger than 1000 (Figure 1B). Because the inside area of the CNPE is coated with carbon, there is a high surface-area-to-volume ratio compared with that of a disk electrode of similar diameter.

Cavity- and Open-Tube-CNPE Comparison. The responses of the CNPEs were tested with FSCV using a typical dopamine waveform of -0.4 to 1.3 V and back at 400 V/s and a scan-repetition frequency of 10 Hz. Figure 2 shows examples of a background-charging-current CV, a background-subtracted CV for 5 μ M dopamine, and the oxidation-current-versus-time response to a bolus of dopamine. Electrodes were equilibrated by applying the waveform in solution for 30 min. The electrodes are very small, as evidenced by the small background-charging currents, which are on the order of 10 nA, not hundreds of nanoamperes, as seen for CFMEs. 4 The CVs have oxidation and reduction peaks that are nearly symmetrical in terms of current, indicating a much better reversibility than traditional CFMEs. The $\Delta E_{\rm p}$ for dopamine is 0.7 V for both cavity and open tube CNPEs, but the peaks are slightly shifted (\sim 0.2 V) to positive potentials. The CVs also have an extra peak at 0.16 V, because of dopamine-cyclization reactions. Scheme 1 shows the oxidation pathway: Following the two-electron oxidation of dopamine (a, DA) to dopamine-o-quinone (b, DOQ), ring closure via deprotonation of the amine side chain to leucodopaminechrome (c, LDAC) occurs irreversibly. LDAC is then oxidized to dopaminechrome (d, DAC). The extra peak at 0.16 V is due to the oxidation of LDAC to DAC and is not typically observed with CFMEs at low concentrations. However, cyclization reactions have been observed with long-length CNTs, which can trap the produced species.²⁷ Here, the CNPE traps the DOQ and increases its local concentration in the cavity, which also amplifies the second redox reaction.

The temporal resolution is key for the application of CNPEs using FSCV. The rise time of the cavity CNPE to a bolus injection of dopamine is not different from that of a CFME ($t_{10-90\%}=1.5\pm0.1$ s for CNPE vs 1.2 ± 0.1 s for CFME, unpaired t test, p=0.2454, n=5), so these electrodes are feasible for rapid measurements using FSCV. The rise time for the opentube electrode is much longer ($t_{10-90\%}=7$ s in Figure 2F,

Cavity CNPEs

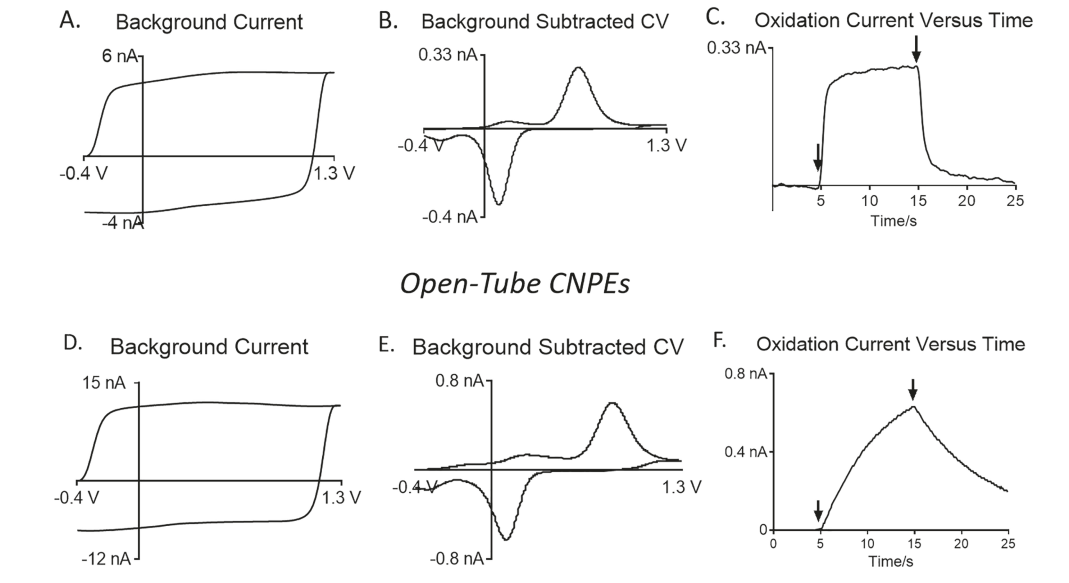


Figure 2. Electrochemical response to $5 \mu M$ dopamine in (A–C) cavity CNPEs and (D–F) open-tube CNPEs. Measurements were obtained at a scan rate of 400 V/s and a scan-repetition frequency of 10 Hz. (A,D) Background currents in PBS buffer, (B,E) background-subtracted cyclic voltammograms for $5 \mu M$ dopamine, and (C,F) measured oxidation current versus time for a flow-injection-analysis experiment. The dopamine-bolus injection and reversion to PBS buffer are marked with black arrows.

Scheme 1. Dopamine-Oxidation Scheme

unpaired t test, p < 0.0001), because of the limited mass transfer in the "infinitely long" shaft. In fact, the open-tube CNPE never reaches equilibrium; the signal increases with time as the solution continues to wick into the CNPE (Figure S1 shows i vs t curves taken every 5 min). Past studies have shown a recessed tip with a large depth-to-orifice ratio leads to a slow temporal response when using FSCV because the analyte gets trapped. Although back pressure can be applied to the electrode to limit the solution front, this is experimentally challenging and not practical for in vivo measurements. Thus, we chose to proceed with the cavity electrode instead, which has a controlled size, shorter equilibration time, and faster temporal response.

Electrochemical Characterization of Cavity CNPEs. The electrochemical characteristics of the cavity CNPEs were compared with those of traditional CFMEs and the conical CNPEs tested previously (Table 1).¹⁵ Conical CNPEs have 200-400 nm tip radii with 150 μ m lengths, whereas CFMEs have 7 μ m tip radii with 100 μ m lengths. Both the dopamineoxidation current and the background-charging current are significantly smaller with the cavity CNPEs than with the other electrodes because the surface area is much smaller (unpaired t tests, $p \le 0.0001$ for both comparisons). A measure of signal per unit area is the oxidation-current-to-background-current ratio, with a larger ratio being better. Cavity CNPEs have a significantly larger ratio than conical CNPEs (unpaired t test, $p \le 0.001$) but a smaller ratio than CFMEs (unpaired t test, $p \le$ 0.0001). The carbon structure of CNPEs is more graphitic and has fewer surface defects and oxide groups than CFMEs, 30,31 so the CNPEs likely adsorb less dopamine and have lower oxidation-current-to-background-current ratios than the CFMEs.

The limit of detection (LOD) for dopamine at the cavity CNPEs (56 ± 13 nM) is larger than those at the conical CNPEs (25 ± 5 nM, unpaired t test, $p \le 0.05$) and CFMEs (19 ± 4 nM, unpaired t test, $p \le 0.01$). The LOD at the cavity CNPEs is likely to be limited by the system noise. The amplifier and filters on the FSCV system are not designed for picoampere-signal detection, and thus, the noise is proportionally higher for small electrodes. Electronics could be optimized in the future.

The difference between the oxidative and reductive peak potentials ($\Delta E_{\rm p}$) of the cavity CNPEs falls between those of the other two electrodes: it is smaller than that of CFMEs (unpaired t test, $p \leq 0.01$) and larger than that of conical CNPEs (unpaired t test, $p \leq 0.05$). For the CNPEs, the deposited carbon is amorphous with oxygen-containing functional groups of about $-0.01~{\rm C/m^2}.^{32}$ The larger $\Delta E_{\rm p}$ of the cavity CNPEs compared with that of the conical CNPEs might be due to their different geometry: the mass-transport distance would be longer in the cavity CNPEs because dopamine needs to diffuse into the cavity; thus, $\Delta E_{\rm p}$ would be larger on the basis of the theory of charge transfer at partially blocked surfaces. In addition, the higher impedance of the cavity CNPEs could increase the $\Delta E_{\rm p}$.

The CVs show dopamine-redox-peak potentials that are shifted positively for the cavity CNPEs compared with that of the CFMEs (Figure 2A). The average dopamine-oxidation-peak potential $(E_{p,a})$ and reduction-peak potential $(E_{p,c})$ of the cavity CNPEs are $0.73 \pm 0.03 \text{ V}$ (n = 6) and $0.09 \pm 0.02 \text{ V}$ (n = 6), respectively, which are about 200 mV shifted from those of the CFMEs $(E_{p,a} = 0.49 \pm 0.01 \text{ V}, E_{p,c} = -0.17 \pm 0.01 \text{ V}, n = 6,$ unpaired *t* test, $p \le 0.0001$ for both comparisons). The potential shift in the oxidation-reduction peaks is due to excess surface charges on the carbon layer, originating from the deprotonation of surface functional groups. Modeling of the double layer at the carbon-nanopipette surface in Figure S2 shows an open-circuit diffuse layer potential of -15 mV. Although that is not as large as the observed shifts, it predicts that the surface does have a negative charge. Potential shifts have also been observed with materials with high amounts of oxygen-containing functional groups, ^{28,34} and the cavity geometry of the negatively charged carbon in the CNPEs could lead to a more predominant effect. In this case, extra voltage needs to be applied for dopamine redox.2,28

Detection of Dopamine at Cavity CNPEs and Numerical Simulation. CNPEs have enhanced dopamine currents and better reversibility because the negative charge of the surface preconcentrates dopamine, and the small cavity traps dopamine, acting like a thin-layer electrochemical cell. Modeling shows the DA concentration near the carbon surface could be 1.5 times higher than its bulk value because of electrostatic interactions and adsorption (Figure S2C). Therefore, higher than expected currents are obtained with CNPEs for dopamine detection, because more dopamine is trapped. The CNPEs are also more reversible, as the oxidation—reduction-currents ratio $(i_{p,a}/i_{p,c})$ of

Table 1. Comparison of Dopamine Detection at Cavity CNPEs, Conical CNPEs, and CFMEs^a

	i_{BG} (nA)	$i_{p,a}$ (nA)	$i_{\mathrm{p,a}}/i_{\mathrm{BG}}$ ratio	LOD (nM)	$\Delta E_{\mathrm{p}} \left(\mathrm{V} \right)$	$i_{\mathrm{p,a}}/i_{\mathrm{p,c}}$
cavity CNPE $(n = 5)$	5.7 ± 0.5	0.19 ± 0.02	0.0326 ± 0.004	56 ± 13	0.62 ± 0.03	1.18 ± 0.09
conical CNPE ¹⁵ $(n = 8)$	$410 \pm 80****$	$14 \pm 3****$	$0.0246 \pm 0.009***$	$25 \pm 5*$	0.52 ± 0.01 *	$1.40 \pm 0.10***$
CFME $(n = 6)$	$570 \pm 160****$	$19 \pm 2****$	$0.0463 \pm 0.010****$	$19 \pm 4**$	$0.67 \pm 0.01**$	$1.59 \pm 0.03****$

^aAll values for 1 μM dopamine detection. Electrochemical measurements were performed with an FSCV waveform scanning from −0.4 to 1.3 V and back at 400 V/s with a scan-repetition frequency of 10 Hz. Significant difference from cavity-CNPE values are shown with asterisks: $p \le 0.05$, ** $p \le 0.01$, *** $p \le 0.001$, **** $p \le 0.0001$ (unpaired t tests).

cavity CNPEs is significantly smaller than that of the CFMEs (Table 1, unpaired t test, $p \le 0.0001$). In our previous work, we demonstrated that a rough surface with a crevice depth >1900 nm traps redox molecules, amplifies the signals, and makes them more reversible. From numerical simulations, cavity CNPEs have a larger current than conical CNPEs because of the redox cycling (Figure S3).

Numerical simulations were used to understand the redox processes and concentration of dopamine in the CNPE during FSCV. Figure 3 shows the waveform, with points marked at

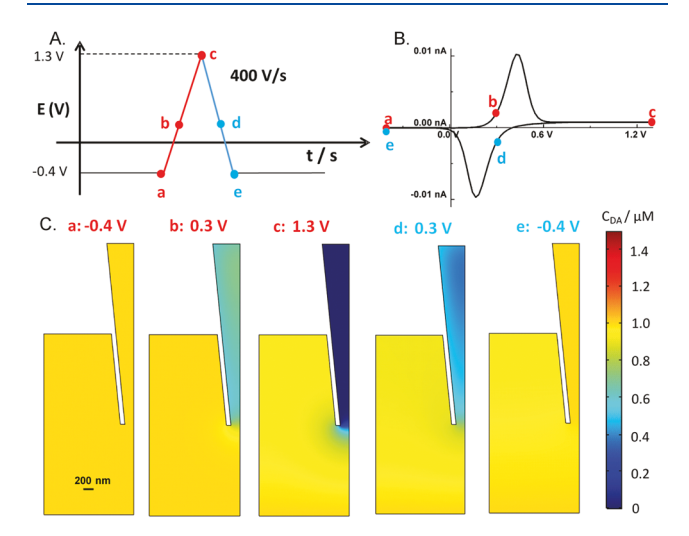


Figure 3. Numerical simulation of dopamine-oxidation—reduction with the cavity CNPEs. (A) FSCV waveform showing potentials where concentrations were modeled. (B) Modeled cyclic voltammogram for dopamine. Symmetric peaks show the thin-layer cell effects. (C) Modeled concentrations of dopamine inside the CNPE. The rectangle is the reservoir of 1 μ M dopamine. Half of a CNPE is shown. On the anodic ramp, at 0.3 V dopamine starts to be oxidized, and by 1.3 V, there is complete oxidation of all DA in the CNPE. On the cathodic ramp, at 0.3 V dopamine is being reformed by reduction, and by -0.4 V, all of the dopamine has been redox-recycled back from dopamine-o-quinone. For all simulations, the scan rate is 400 V/s, σ is -0.01 C/m², the radius is 200 nM, and H is 20.

several potentials. A simulated CV is also shown, with the points also marked. Although the real experimental geometry and electron-transfer processes are likely much more complicated (i.e., because of porous carbon structure and unknown surfacecharge density and because they are adsorption-controlled and functional-group-dependent), we still observe similar oxidation-reduction peaks in the simulated voltammogram. The bottom of Figure 3 shows simulations of the concentration of dopamine in the CNPE at each voltage. When dopamine is oxidized starting at 0.3 V, the concentration at the carbon surface decreases. At 1.3 V, all the dopamine is depleted in the CNPE. At 0.3 V on the anodic scan, dopamine is being reformed as dopamine-o-quinone is reduced back to dopamine. When the potential hits -0.4 V at the end of the scan, all of the dopamine has been regenerated from dopamine-o-quinone, making the cavity concentration the bulk dopamine concertation. Thus, in a cavity CNPE, dopamine is rapidly oxidized but rapidly redoxrecycled during an FSCV scan. These simulations are for a cavity electrode, but note that the surface potential and DAconcentration profile near the tip region would be the same for the cavity and open-tube CNPEs.

The cavity geometry enhances the electric field at the tip, which enables stronger electrostatic attraction for positively charged dopamine during the holding potential. One piece of experimental evidence supporting the fact that the electric field is enhanced is that the signal at the cavity CNPEs is not dependent on the switching potential. For CFMEs, Figure 4A

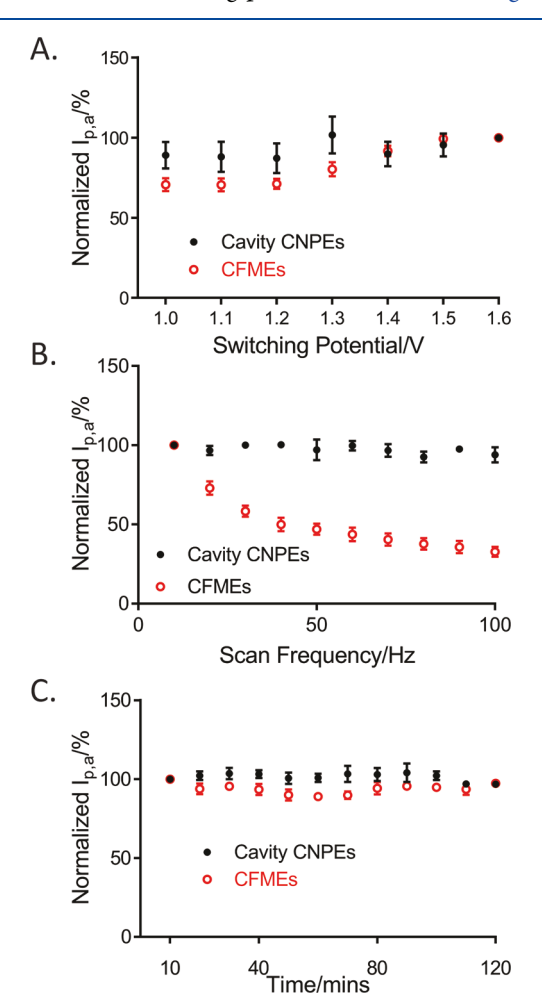


Figure 4. (A) Effect of switching potential. The plot shows the average oxidation current for 1 μ M dopamine at the cavity CNPEs (black dots, n=5) and CFMEs (red circles, n=5) for each switching potential (1.0 to 1.6 V, with an interval of 0.1 V) with a triangle waveform from -0.4 and a 400 V/s scan rate. Peak currents were normalized to the current using the 1.6 V waveform. (B) Effect of the scan-repetition frequency. The plot shows the peak oxidation current of the cavity CNPEs (black dots, n=4) and CFMEs (red circles, n=5) with a -0.4 to 1.3 V waveform and a scan rate of 400 V/s. Peak currents were normalized to the current at 10 Hz. (C) Two-hour stability test of cavity CNPEs (black dots, n=3) and CFMEs (red circles, n=3) with constant waveform application (-0.4 to 1.3 V, 400 V/s, 10 Hz). The oxidation current to 1 μ M dopamine was normalized to the signal observed after 10 min of equilibration. The error bars are the standard error of the mean.

shows that oxidative current is higher after a switching potential of 1.3 V, which is sufficient to break carbon bonds and renew the surface. In contrast, the oxidative current does not change for cavity CNPEs with switching potentials of 1.0 to 1.6 V (one-way ANOVA, Bonferroni post-test, p = 0.2906). The enhanced electric field at the tip causes oxidation of carbon even at lower potentials, so there is no effect from the switching potential.

The trapping effect at the nanocavity creates thin-layer cell-like conditions that lead to other properties, such as an FSCV-waveform frequency-independent response. Figure 4B shows the dopamine-oxidation current with scan-repetition frequencies from 10 to 100 Hz, and the current does not significantly change with increasing scan frequency (one-way ANOVA, Bartlett's test, p=0.4542). In comparison, the oxidation-current drop is dramatic at CFMEs, with approximately 50% signal loss at 50 Hz and 67% loss at 100 Hz compared with at 10 Hz. In addition, the rise time (t_{10-90}) is not different at different scanning frequencies $(t_{10-90}=1.5\pm0.1~{\rm s}$ at 10 Hz vs $1.7\pm0.2~{\rm s}$ at 100 Hz, paired t test, p=0.4432, n=3). The frequency-independent property enables highly sensitive neurotransmitter detection at rapid repetition frequencies.

Stability and Selectivity Tests. Electrodes are typically used in vivo for hours at a time to measure neurotransmission, and typical experiments in *Drosophila* are up to 2 h long. ³⁶ Figure 4C shows the dopamine-oxidation signal is constant for 2 h of continuous scanning with CNPEs (one-way ANOVA, Bartlett's test, p > 0.05, n = 3), the same as with traditional CFMEs. Given the enhanced electric fields that may break carbon bonds, it is very promising that these electrodes are stable for 2 h (1200 FSCV scans).

Ascorbic acid (AA) is a common anionic interfering agent in extracellular fluid, and the selectivity of the cavity CNPEs for dopamine over AA was tested. ^{37–39} Figure 5A shows the CV for

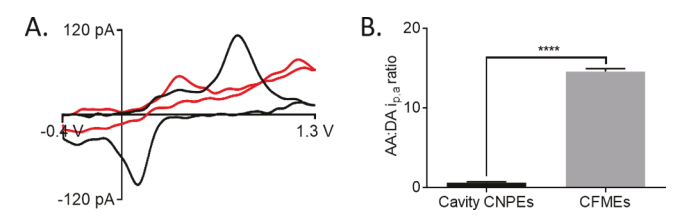


Figure 5. (A) CVs of 200 μ M ascorbic acid (red line) and 1 μ M dopamine obtained from the same cavity CNPE and CFME. (B) Column plots showing the oxidation-current ratio for 200 μ M ascorbic acid to dopamine at the cavity CNPEs (black, n = 5) and CFMEs (gray, n = 5). The oxidation-current ratio at the cavity CNPEs is significantly smaller than that at the CFMEs for the measurement of ascorbic acid (t test, $p \le 0.0001$).

200 μ M AA and 1 μ M DA, and the peak for AA is much smaller than that for dopamine, even though AA is at a higher concentration. The ascorbic acid to dopamine oxidation current ratio is 0.6 ± 0.1 (n = 5) at the cavity CNPEs, which is significantly lower than that at the CFMEs (14.6 \pm 0.4, n = 5, ttest, $p \le 0.0001$), indicating dramatically improved dopamine selectivity over ascorbic acid at the cavity CNPEs (Figure 5B). Previously, different nanomaterials, polymers, surface modifications, and electrochemical techniques have been used to improve the selectivity. 34,40-42 Here, the cavity geometry and the resulting enhanced electric field at the tip preconcentrates dopamine (Figure S1) and repels negatively charged species such as ascorbic acid. In addition, ascorbic acid has no obvious reduction, 43 indicating an irreversible reaction at the cavity CNPEs, which is different from the reversible reaction at the CFMEs. 34,41,44 Thus, there is no redox cycling for ascorbic acid as there is with dopamine. The promising dopamine selectivity over ascorbic acid is due to both the repulsion by the negative electric field and the irreversible redox reaction.

Measurement of Dopamine in Mouse-Brain Slices. To test the stability and robustness for tissue measurements, the

cavity CNPEs were tested in mouse-brain slices with dopamine exogenously applied to the tissue. Because the cavity CNPEs are open to their environment, there was a concern that they could be clogged with tissue. Figure 6A shows that the CNPE is able to

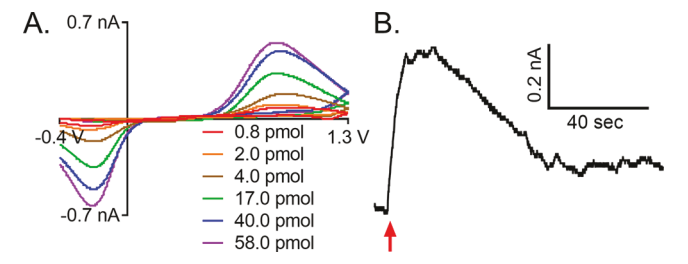


Figure 6. Electrochemical response of cavity CNPEs to exogenous dopamine application. Measurements were obtained at a scan rate of 400 V/s and at a scan-rate frequency of 10 Hz. (A) Background-subtracted CVs of the same electrode with varying times of dopamine application (pressure kept constant). The pressure-ejection times (0.02 to 1.5 s) were converted to the molar quantities released by the picospritzing pipet using the initial concentration of the dopamine solution (150 μ M) and the volume of solution released for each duration. (B) Oxidative current versus time for a different electrode with a 1 s puff of dopamine (27.0 pmol). The dopamine was ejected at the arrow.

detect dopamine in tissue, with different currents for different amounts of dopamine applied; both the primary-oxidation and -reduction peaks are present in the background-subtracted CVs. The $\Delta E_{\rm p}$ increased compared with values obtained from the flow-injection system (Table 1). This increase is a known phenomenon in tissue measurements that is likely due to the adsorption of biomolecules to the electrode, which subsequently impedes electron transfer. In Figure 6B, the oxidative-current-versus-time plot shows that the dopamine signal decreases after the ejection, demonstrating that the analyte is able to exit the cavity. These results indicate that the cavities of the CNPEs are not being clogged when inserted into tissue, and they are able to detect the presence of dopamine in tissue.

CONCLUSIONS

Cavity CNPEs are useful nanoelectrodes for detection of dopamine with submicrometer spatial resolution. There are two main effects that lead to desirable electrochemical properties: analyte trapping and an enhanced electric field. First, the small cavity of CNPEs traps dopamine, allowing exhaustive redox cycling and leading to high sensitivity because the DA concentrations are much higher than the bulk value. The trapping effect also leads to the appearance of secondary peaks because of the cyclization of oxidation products and an FSCV frequency-independent response. Second, the enhanced electric field at the tip gives rise to enhanced selectivity over ascorbic acid and a response that is independent of the switching potential. CNPEs can be used in tissue for dopamine and thus are robust enough to be implanted in tissue. These CNPEs are truly nanometer in width and should be useful for measurements in discrete locations, including in small model systems, at synapses, and on living cells.

ASSOCIATED CONTENT

S Supporting Information

The Supporting Information is available free of charge on the ACS Publications website at DOI: 10.1021/acs.analchem.8b05885.

FSCV response to 1 μ M dopamine in an open-tube CNPE, numerical simulations of double layers and preconcentration in the CNPE tip, comparison of response simulations of a conical nanofiber and a cavity nanopipette, and supplemental methods for the finite element simulation of CNPEs for dopamine detection (PDF)

AUTHOR INFORMATION

Corresponding Author

*E-mail: jventon@virginia.edu. Tel.: 434-243-2132.

ORCID ©

Cheng Yang: 0000-0001-5635-8181 Dengchao Wang: 0000-0002-4909-7830 B. Jill Venton: 0000-0002-5096-9309

Notes

The authors declare no competing financial interest.

ACKNOWLEDGMENTS

This work was funded by NIH grants R01EB026497 (B.J.V. and M.V.M.) and NIHR01MH085159 (B.J.V.) and NSF grant CHE-1763337 (M.V.M.).

REFERENCES

- (1) Ambrosi, A.; Pumera, M. Chem. Soc. Rev. 2016, 45, 2740.
- (2) Runnels, P. L.; Joseph, J. D.; Logman, M. J.; Wightman, R. M. Anal. Chem. 1999, 71 (14), 2782–2789.
- (3) Chen, P.; McCreery, R. L. Anal. Chem. 1996, 68 (22), 3958-3965.
- (4) Yang, C.; Denno, M. E.; Pyakurel, P.; Venton, B. J. Anal. Chim. Acta 2015, 887, 17–37.
- (5) Özel, R. E.; Wallace, K. N.; Andreescu, S. Anal. Chim. Acta 2011, 695 (1), 89–95.
- (6) Makos, M. A.; Kim, Y.-C.; Han, K.-A.; Heien, M. L.; Ewing, A. G. Anal. Chem. **2009**, 81 (5), 1848–1854.
- (7) Shin, M.; Field, T. M.; Stucky, C. S.; Furgurson, M. N.; Johnson, M. A. ACS Chem. Neurosci. 2017, 8 (9), 1880–1888.
- (8) Li, Y.-T.; Zhang, S.-H.; Wang, L.; Xiao, R.-R.; Liu, W.; Zhang, X.-W.; Zhou, Z.; Amatore, C.; Huang, W.-H. *Angew. Chem., Int. Ed.* **2014**, 53 (46), 12456–12460.
- (9) Koehne, J. E.; Marsh, M.; Boakye, A.; Douglas, B.; Kim, I. Y.; Chang, S.-Y.; Jang, D.-P.; Bennet, K. E.; Kimble, C.; Andrews, R.; Meyyappan, M.; Lee, K. H. *Analyst* **2011**, *136* (9), 1802–1805.
- (10) Strein, T. G.; Ewing, A. G. Anal. Chem. 1992, 64 (13), 1368–1373.
- (11) Shen, M.; Colombo, M. L. Anal. Methods 2015, 7 (17), 7095–7105.
- (12) Morris, C. A.; Friedman, A. K.; Baker, L. A. Analyst 2010, 135 (9), 2190–2202.
- (13) Clausmeyer, J.; Schuhmann, W. TrAC, Trends Anal. Chem. 2016, 79, 46–59.
- (14) Mirkin, M. V.; Nogala, W.; Velmurugan, J.; Wang, Y. Phys. Chem. Chem. Phys. **2011**, 13 (48), 21196–21212.
- (15) Rees, H. R.; Anderson, S. E.; Privman, E.; Bau, H. H.; Venton, B. J. Anal. Chem. **2015**, 87 (7), 3849–3855.
- (16) Yu, Y.; Noël, J.-M.; Mirkin, M. V.; Gao, Y.; Mashtalir, O.; Friedman, G.; Gogotsi, Y. Anal. Chem. 2014, 86, 3365–3372.
- (17) Arrigan, D. W. M. Analyst 2004, 129 (12), 1157-1165.

- (18) Takahashi, Y.; Shevchuk, A. I.; Novak, P.; Murakami, Y.; Shiku, H.; Korchev, Y. E.; Matsue, T. J. Am. Chem. Soc. 2010, 132 (29), 10118–10126.
- (19) Schrlau, M. G.; Brailoiu, E.; Patel, S.; Gogotsi, Y.; Dun, N. J.; Bau, H. H. Nanotechnology 2008, 19 (32), 325102.
- (20) Schrlau, M. G.; Dun, N. J.; Bau, H. H. ACS Nano 2009, 3 (3), 563-568.
- (21) Li, Y.; Hu, K.; Yu, Y.; Rotenberg, S. A.; Amatore, C.; Mirkin, M. V. J. Am. Chem. Soc. **2017**, 139 (37), 13055–13062.
- (22) Bucher, E. S.; Wightman, R. M. Annu. Rev. Anal. Chem. 2015, 8, 239–261
- (23) Strand, A. M.; Venton, B. J. Anal. Chem. 2008, 80 (10), 3708–3715.
- (24) Schrlau, M. G.; Falls, E. M.; Ziober, B. L.; Bau, H. H. Nanotechnology 2008, 19 (1), 015101.
- (25) Hu, K.; Wang, Y.; Cai, H.; Mirkin, M. V.; Gao, Y.; Friedman, G.; Gogotsi, Y. Anal. Chem. **2014**, 86 (18), 8897–8901.
- (26) Wilde, P.; Quast, T.; Aiyappa, H. B.; Chen, Y.-T.; Botz, A.; Tarnev, T.; Marquitan, M.; Feldhege, S.; Lindner, A.; Andronescu, C.; Schuhmann, W. ChemElectroChem 2018, 5 (20), 3083–3088.
- (27) Muguruma, H.; Inoue, Y.; Inoue, H.; Ohsawa, T. J. Phys. Chem. C **2016**, 120 (22), 12284–12292.
- (28) Yang, C.; Wang, Y.; Jacobs, C. B.; Ivanov, I.; Venton, B. J. Anal. Chem. **2017**, 89, 5605–5611.
- (29) Yang, C.; Trikantzopoulos, E.; Nguyen, M. D.; Jacobs, C. B.; Wang, Y.; Mahjouri-Samani, M.; Ivanov, I. N.; Venton, B. J. *ACS Sensors* **2016**, *1*, 508–515.
- (30) Vitol, E. A.; Schrlau, M. G.; Bhattacharyya, S.; Ducheyne, P.; Bau, H. H.; Friedman, G.; Gogotsi, Y. *Chem. Vap. Deposition* **2009**, *15* (7–9), 204–208.
- (31) Roberts, J. G.; Moody, B. P.; McCarty, G. S.; Sombers, L. A. Langmuir **2010**, 26 (11), 9116–9122.
- (32) Wang, D.; Mirkin, M. V. J. Am. Chem. Soc. 2017, 139 (34), 11654–11657.
- (33) Yang, C.; Jacobs, C. B.; Nguyen, M. D.; Ganesana, M.; Zestos, A. G.; Ivanov, I. N.; Puretzky, A. A.; Rouleau, C. M.; Geohegan, D. B.; Venton, B. J. *Anal. Chem.* **2016**, *88*, *645*–*652*.
- (34) Yang, C.; Trikantzopoulos, E.; Jacobs, C. B.; Venton, B. J. *Anal. Chim. Acta* **2017**, *965*, 1–8.
- (35) Takmakov, P.; Zachek, M. K.; Keithley, R. B.; Walsh, P. L.; Donley, C.; McCarty, G. S.; Wightman, R. M. *Anal. Chem.* **2010**, 82 (5), 2020–2028.
- (36) Xiao, N.; Privman, E.; Venton, B. J. ACS Chem. Neurosci. 2014, 5 (8), 666–673.
- (37) Ping, J.; Wu, J.; Wang, Y.; Ying, Y. Biosens. Bioelectron. 2012, 34 (1), 70-76.
- (38) Chen, C.-H.; Luo, S.-C. ACS Appl. Mater. Interfaces 2015, 7, 21931–21938.
- (39) Hočevar, S. B.; Wang, J.; Deo, R. P.; Musameh, M.; Ogorevc, B. *Electroanalysis* **2005**, *17* (5–6), 417–422.
- (40) Peairs, M. J.; Ross, A. E.; Venton, B. J. Anal. Methods 2011, 3 (10), 2379-2386.
- (41) Zestos, A. G.; Yang, C.; Jacobs, C. B.; Hensley, D.; Venton, B. J. *Analyst* **2015**, *140*, 7283–7292.
- (42) Roberts, J. G.; Toups, J. V.; Eyualem, E.; McCarty, G. S.; Sombers, L. A. Anal. Chem. 2013, 85 (23), 11568-11575.
- (43) Ruiz, J. J.; Rodriguez-mellado, J. M.; Dominguez, M.; Aldaz, A. J. Chem. Soc., Faraday Trans. 1 1989, 85 (7), 1567–1574.
- (44) Trikantzopoulos, E.; Yang, C.; Ganesana, M.; Wang, Y.; Venton, B. J. Analyst **2016**, 141 (18), 5256–5260.

NOTE ADDED AFTER ASAP PUBLICATION

This paper published ASAP on March 12, 2019 with an error in the title. The revised paper was reposted on March 15, 2019.